Carbohydrate Polymers 104 (2014) 246–252

Contents lists available at ScienceDirect

Carbohydrate Polymers

journal homepage: www.elsevier.com/locate/carbpol

Pleurotus nebrodensis polysaccharide induces apoptosis in human non-small cell lung cancer A549 cells

Haiyan Cui, Changlu Wang*, Yurong Wang, Zhenjing Li, Yanan Zhang, Mianhua Chen, Fengjuan Li

Key Laboratory of Food Nutrition and Safety, Ministry of Education, School of Food Engineering and Biotechnology, Tianjin University of Science and Technology, Tianjin 300457, China

ARTICLE INFO

Article history:
Received 30 September 2013
Received in revised form
30 December 2013
Accepted 2 January 2014
Available online 9 January 2014

Keywords:
Pleurotus nebrodensis polysaccharides
A549 cells
Anticancer
Apoptosis

ABSTRACT

Polysaccharides derived from edible fungi inhibit the proliferation of tumor cells. In this study, we investigated the effects of a polysaccharide (PN50G) from *Pleurotus nebrodensis* on A549 cell proliferation and apoptosis. MTT assay showed that PN50G induced apoptosis in the A549 cells in a dose-dependent. However, PN50G did not affect the proliferation viability of human fetal lung fibroblast cells MRC-5. Scanning electro microscopy (SEM) results indicate that PN50G induced a typical apoptotic morphological feature in A549. DNA accumulation and fragmentation were determined by acridine orange/ethidium bromide (AO/EB) staining. Flow cytometric analysis demonstrated that PN50G caused A549 cell apoptosis via cell arrest at the S phase. PN50G also extended the comet tail length in single-cell gel electrophoresis and disrupted the mitochondrial membrane potential as determined by Rdamine-123 staining. Further analysis by qRT-PCR showed that the expression of caspase-3 and caspase-9 mRNA increased. These findings suggest that PN50G can inhibit A549 cell proliferation and induce apoptosis mainly by activating the intrinsic mitochondrial pathway.

1. Introduction

Cancer is globally the second most life-threatening disease, and its mortality rate is second only to that of cardiovascular diseases (Xie, Liu, Shen, Nie, & Zhang, 2013). Lung cancer is the leading cause of cancer deaths in men and the second leading cause of cancer deaths in women worldwide (Parkin, 2001). Chemoprevention is an effective way of reducing cancer risk. However, it also frequently exhibits serious side effects (Hanif et al., 1996; Kamesaki, 1998). By contrast, biologically active metabolites found in medicinal mushrooms may provide anti-cancer action with a minimum of side effects (Bremner et al., 2009; Thangam, Suresh, & Asenath Princy, 2013). In particular, numerous polysaccharides isolated from plants, fungi, algae, and animals are ideal candidates for anticancer treatment and can potentially improve cancer immunity (Newman, Cragg, & Snader, 2003; Schepetkin & Quinn, 2006).

Apoptosis or programmed cell death is characterized by a typical cellular morphology and biochemical features, including cell shrinkage, cytoplasmic vacuolization, chromatin condensation, DNA fragmentation, and eventual cellular breakdown into apoptotic bodies (Adrie et al., 2001; Heo et al., 2011). Apoptosis is an important biological mechanism that contributes to the maintenance of the integrity of multicellular organisms and is dependent on the expression of a cell-intrinsic suicide machinery (Vermeulen, Berneman, & Van Bockstaele, 2003). Current research on the effects of polysaccharides on cancer focuses on the impact of apoptosis. Ma et al. identified the anticancer components of *Inonotus obliquus* against human prostatic carcinoma cell PC3 and breast carcinoma cell MDA-MB-231 (Ma, Chen, Dong, & Lu, 2013). Two acidic polysaccharides that are potentially potent antitumor agents for lung tumorigenesis prevention were purified by Xin et al. from *Paeonia tenuifolia* roots (Xin et al., 2012).

Edible mushrooms are a highly nutritious food resource that has tonic and medicinal applications in folk medicine (Bae, Kim, Lee, & Lee, 2011). One of these mushrooms is *Pleurotus nebrodensis*, which is native to China, Southern Europe, and Central Asia (Miyazawa, Okazaki, & Ohga, 2008). However, few studies have focused on *P. nebrodensis* polysaccharides and their bioactivities. In our previous study (Wang et al., 2013), PN50G was purified from *P. nebrodensis* and was confirmed to be nontoxic.

The current study aims to determine the apoptotic effects of the water-soluble polysaccharide PN50G from *P. nebrodensis* and to identify the biochemical mechanisms underlying the apoptotic induction in the human cancer cell line A549. The induction of apoptotic body formation was investigated via AO/EB staining and flow cytometry. The regulation of caspase-3 and caspase-9 mRNA

* Corresponding author at: School of Food Engineering and Biotechnology, Tianjin University of Science and Technology, No. 29, 13th Avenue, TEDA, Tianjin 300457, China.
E-mail addresses: clw123@tust.edu.cn, haiyancui2010@163.com (C. Wang).

0144-8617/$ – see front matter © 2014 Elsevier Ltd. All rights reserved.
http://dx.doi.org/10.1016/j.carbpol.2014.01.001

expression in A549 cells treated with *P. nebrodensis* polysaccharides was also investigated. To the best of our knowledge, this study is the first to evaluate the anticancer potential of edible *P. nebrodensis*. In addition to its nutritional properties, PN50G is a highly promising candidate polysaccharide for the development of anticancer medicines.

2. Materials and methods

A549 (the human non-small cell lung cancer) cells and non-tumor MRC-5 cell line were obtained from the Bioresource Collection and Research Center of the Food Industry Research and Development Institute (Hsinchu, Taiwan, ROC). F12 medium was purchased from Thermo (Beijing, China). Fetal bovine serum (FBS) was obtained from Gibco GRL (Grand Island, NY, USA). Penicillin–streptomycin solution, trypsin, phosphate buffered saline (PBS), dimethyl sulfoside side (DMSO), 3-(4,5-dimethylthiazol-2-yl)-2,5-diphenyltertrazolium bromide (MTT), low-melting point agarose, normal-melting point agarose, and cell lysis solution were purchased from Solarbio (Beijing, China). Propidium iodide (PI), Rhodamine 123, AO/EB were purchased from Sigma–Aldrich (St. Louis, MO, USA). RNeasy Mini Kit was purchased from Qiagen (Hilden, Germany). The PrimeScript 1st Strand cDNA Synthesis Kit was obtained from Takara Bio (Dalian, China). The SYBR Green PCR master mix was purchased from Invitrogen (Shanghai, China).

2.1. Isolation and purification of the PN50G polysaccharide

The PN50G polysaccharide was extracted from fresh *P. nebrodensis* by decoction and alcohol sedimentation techniques. Briefly, the mushrooms were ground and mixed with distilled water at a grain: water ratio of 1:20 (w/v). The mixture was incubated three times in a water bath at 100 °C with stirring for 4 h. After extracted, the mixture was cooled to room temperature (25 ± 2 °C), filtered through a gauze and centrifuged at 4000 r/min for 15 min. The supernatant was collected, concentrated with a rotary evaporator, precipitated with four volumes of 50% ice-cold ethanol, and freeze-dried (Thermo Scientific, Rockford, IL, USA). The crude polysaccharide was further purified through Sepharose 4B gel permeation column (60 cm × 2.6 cm) with ultrapure water as eluent using the Automated Fraction Collector. A main single fraction was obtained (PN50G) and was then collected and freeze-dried. The molecular mass of PN50G was determined to be 200 kDa by gel filtration. The percentage of total protein and carbohydrate constituent were determined to be 2.6 ± 0.9% and 92.4 ± 6.1% (w/w) by the phenol–sulfuric acid and Bradford's method (Wang et al., 2013). The component sugars of PN50G were determined by gas chromatography (GC). The polysaccharide were hydrolyzed with acid, reduced and acetylated, indicating that the neutral sugar components were xylose, mannose, glucose, galactose, and a molar ratio of 1:2.7:34.4:1.5, with a trace of arabinose (Fig. 1B). Using Fourier transform infrared spectroscopy (FTIR) (Bruker, Ettlingen, Germany) (Fig. 1C), the structure of PN50G was determined to possess a backbone composed of α-D-glucopyranosyl (Glcp) residues. Ultraviolet spectrophotometry (Agilent Santa Clara, CA, USA) confirmed the absence of nucleic acid.

2.2. Cell culture

The non-small cell lung cancer A549 cell line and human fetal lung fibroblast cells MRC-5 cell line were routinely cultured in our laboratory. The cell lines were grown and maintained in F12 medium supplemented with 10% fetal bovine serum and 1× penicillin/streptomycin (100 U/mL P + 0.1 mg/mL S) at 37 °C in a 5% CO_2 atmosphere. After the cells were grown to 90% confluence in a T25 tissue culture flask (TPP Biochrom AG, Trasadingen, Switzerland), they were plated at a density of 1×10^6 or 8×10^3 cells/mL in the 6-well plates or 96-well plates to perform the following bio-assay. The plate was incubated at 37 °C for overnight to allow cell attachment to the bottom. After the cell supernatant was removed, an aliquot with equal volume of test sample was added to the well.

2.3. Cell viability and proliferation

The cell viabilities of MRC-5 cell and A549 cell treated with PN50G at different concentrations were determined by MTT (Lee, Yoon, & Park, 2008) assay to evaluate the possible cytotoxic effects of the test samples. MRC-5 cell and A549 cell in the absence or presence of samples at different concentrations (100 μL/well) were cultured in 96-well plates for 48 h. Aliquots of 20 μL of 5 mg/mL MTT in PBS were added to each well in the 96-well plate. The plates were incubated for another 4 h and centrifuged. The culture medium was then discarded. The plates were washed carefully twice with PBS buffer. Aliquots of 150 μL of DMSO were added to each well and oscillated for 15 min to extract the insoluble formazan that formed. The absorbance was measured at 570 nm on a plate reader (ELISA reader, ASYS Hitech, GmbH, Austria). MRC-5 cell and A549 cell viability were calculated as:

$$\text{Survival}\ \ (\%) = A/B \times 100\%$$

where *A* is the average optical density of the PN50G-treated cells, *B* is the average optical density of the control wells (culture medium with cells).

2.4. Apoptosis assessment by AO/EB staining

PN50G-induced apoptosis in A549 cells was measured by using AO/EB staining assay, which is based on the difference in membrane integrity between necrotic and apoptosis. A549 cells were incubated in the absence or presence of PN50G at 37 °C and 5% CO_2 for 48 h. The cells were washed 3 times with PBS and fixed with 4% paraformaldehyde for 10 min at 4 °C. Then, cell culture was stained with AO/EB solution (100 μg/mL AO and 100 μg/mL EB in PBS) at room temperature in the dark. The cells were observed under an inverted fluorescence microscope (AMG, USA).

2.5. Morphologic observations

A549 cells (1×10^6 cells/mL) were grown on cover slips in 6-well plates and treated with PN50G at different concentrations for 48 h. The morphological changes were observed under a SEM (Hitachi, Tokyo, Japan).

2.6. Measurement of DNA damage by the comet assay

DNA damage (caused by apoptosis) was evaluated by alkaline single cell gel electrophoresis (comet assay). The PN50G treated and untreated cells were plated at a density of 1×10^5 cells per dish and left to adhere overnight. The cells were then trypsinized, resuspended in PBS and counted. 0.5% normal agarose in PBS (100 μL) prewarmed at 45 °C was dropped onto the slides and covered with a glass coverslip. The coverslips were removed after allowing the agarose to set at 4 °C for 10 min. Then, 10 μL of the cells were mixed with 75 μL of 0.7% low melting point agarose in PBS at 37 °C, spread onto the slides, and left for 10 min at 4 °C. A final layer of 75 μL of 0.7% low melting point agarose was applied in the same way. The slides from which the coverslips had been removed were immersed in chilled lysis buffer containing 10% DMSO at 4 °C for 2 h, then placed in electrophoresis buffer (1 mmol/L of EDTA, 300 mmol/L of NaOH, pH > 13) in a tank at 4 °C for 40 min to allow alkaline

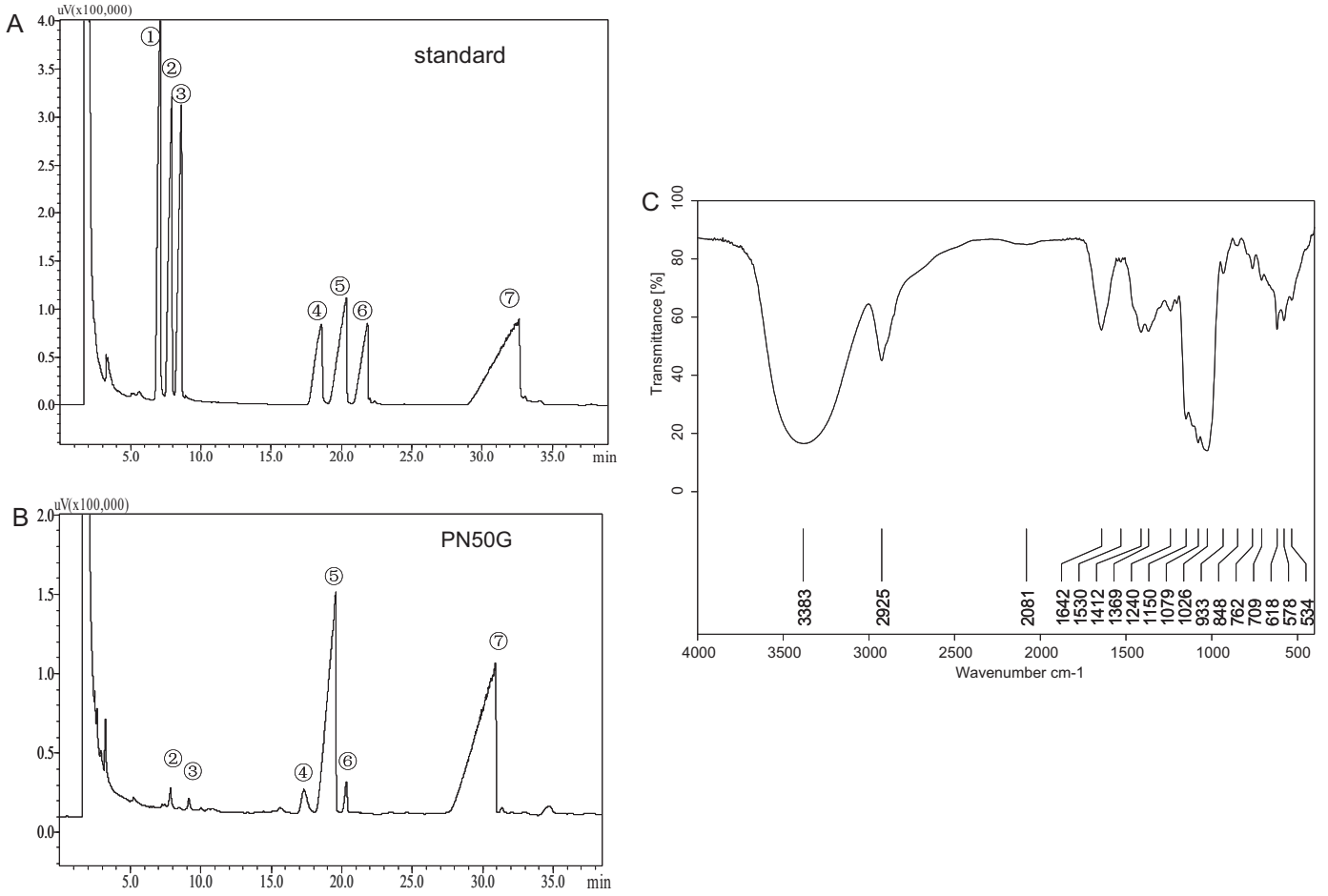

Fig. 1. (A) Gas chromatograms of the standard monosaccharides: (1) ribose (Rib); (2) arabinose (Ara); (3) xylose (Xyl); (4) mannose (Man); (5) glucose (Glu); (6) galactose (Gal); (7) inositol. (B) Gas chromatograms of the monosaccharides derived from PN50G. (C) FTIR spectrum (in KBr) of *p.nebrodensis* polysaccharides PN50G.

unwinding of the DNA. Electrophoresis was performed for 20 min at 25 V and 300 mA. The slides were then transferred to 0.4 mmol Tris-buffer (pH 7.5), washed three times and gently dried. Comets were stained with propidium iodide (2 μg/mL) and analyzed by confocal laser scanning microscopy (Nikon, Tokyo, Japan). Image analysis and tail length analysis were performed with CASP 1.2.2 software (CaspLab, Germany), and 20 cells were randomly selected per sample.

2.7. Cell cycle analysis

A549 cells (1×10^6 cells/mL) were seeded in 100 mm dishes and exposed to PN50G (0, 50, 100 and 200 μg/mL). The cells were washed in PBS and collected by trypsinization, fixed in 70% glacial ethanol, washed in PBS, resuspended in 1 mL of PBS containing 50 U/mL RNase and 50 μg/mL PI, and then incubated for 40 min in the dark at 4 °C. Cell cycle analysis was performed by flow cytometry (BD, Franklin Lakes, NJ, USA), and the population of cells in each phase was calculated using the Modifit LT software program. Each experiment was conducted three times.

2.8. Analysis of mitochondrial potential ($\Delta\Psi_m$)

Changes in mitochondrial membrane potential ($\Delta\Psi_m$) due to mitochondrial dysfunction were detected using rhodamine-123 (Lemasters & Nieminen, 1997). Briefly, A549 cells (1×10^5 cells/mL) were incubated in the absence or presence of PN50G (50, 100 and 200 μg/mL) in 100 mm dishes. The cells were trypsinized and washed with PBS, and then incubated at 37 °C for 10 min with rhodamine-123 (5 μg/mL). Finally, the cells were washed twice in PBS and observed by an inverted fluorescence microscope (AMG, USA). Each image shown is representative of 20 randomly observed fields.

2.9. qRT-PCR

Cells were harvested after cultivation. Total RNA was extracted using the RNeasy Mini-Kit according to the manufacturer's protocol. First-strand cDNA was synthesized using the PrimeScript 1st Strand cDNA Synthesis Kit, with the Oligo dT-Adaptor Primer. Gene expression was monitored by qRT-PCR, carried out using the SYBR Green PCR master mix. Primers for Caspaes-3, Caspase-9 and β-Actin gene were designed (Table 1). qRT-PCR was performed using

Table 1
Sequences of gene-specific qRT-PCR primers.

Gene	Sequence of primers (upstream) (downstream)
Casp-3	TGTGAGGCGGTTGTAGAAGTT CGCTTCCATGTATGATCTTTGGTT
Casp-9	TGGAGACTCGAGGGAGTCAG TCGACAACTTTGCTGCTTGC
β-Actin	AACTGGAACGGTGAAGGTGA GTGCAATCAAAGTCCTCGGC

the ABI step one plus system (applied biosystems) followed by melting curve analysis with the following cycling program: initial activation at 95 °C for 10 min, followed by 40 cycles of denaturation at 95 °C for 30 s, annealing at 55 °C for 1 min, and extension at 72 °C for 1 min.

2.10. Statistical analysis

Each experiment was repeated at least three times. Numerical data are presented as mean ± sem. The difference between means was analyzed by using one-way ANOVA. All statistical analyses were performed by using SPSS 17.0 software (Chicago, IL, USA). $P < 0.05$ was considered significant.

3. Results

3.1. Effect of PN50G on A549 cell inhibition

An in vitro anticancer assay was conducted using A549 cell reduction and with the nontumor MRC-5 cells as control to test the antitumor activity of PN50G. The effects of PN50G treatment on the proliferation of MRC-5 and A549 cells varied (Fig. 2). The MRC-5 cells treated with 25 μg/mL–400 μg/mL PN50G showed no statistical differences with those without PN50G (Fig. 2A). After the A549 cells were treated with 25 μg/mL–400 μg/mL PN50G for 48 h, the inhibitory percentage against cancer cell proliferation was determined. The effects of various PN50G concentrations on A549 cell viability are shown in Fig. 2B. PN50G strongly inhibited A549 cell proliferation in a dose-dependent manner. PN50G became cytotoxic at 50 μg/mL, and no significant differences were found between the two high levels (200 and 400 μg/mL). Thus, 48 h PN50G treatments at 50, 100, and 200 μg/mL were used in the subsequent experiments.

3.2. PN50G-induced apoptosis in A549 cells as determined by morphological observations

After treatment with or without PN50G for 48 h, the morphology of the A549 cells was determined by SEM. Cytotoxicity assays showed different profiles, which indicate statistically significant differences between the treated cells and the controls. As shown in Fig. 3A, numerous microvilli remained intact on the surface of the control group cells. Typical apoptotic morphological changes such as cell shrinkage, membrane blebbing, cytoplasmic vacuolization, and micronucleus formation, which are characteristic of apoptosis in response to PN50G treatment, were observed in the A549 cells in a concentration-dependent manner. This result suggests that PN50G induces apoptosis in A549 cells.

Table 2
Effect of PN50G on cell cycle distribution and apoptosis rate of A549 cells ($n = 3$).

PN50G (μg/mL)	Apoptosis (%)	G_0/G_1 (%)	S (%)	G_2/M (%)
0	0.25 ± 0.03	72.34 ± 3.03	15.77 ± 0.69	11.89 ± 0.43
50	2.39 ± 0.01	65.38 ± 4. 65	21.93 ± 0.51	11.70 ± 0.62
100	17.52 ± 0.12	53.82 ± 2.18	24.01 ± 1.18	5.18 ± 0.29
200	30.33 ± 0.06	33.07 ± 2.04	36.92 ± 0.82	0.00 ± 0.00

3.3. Apoptotic effect of PN50G on A549 cells

Necrotic and apoptotic cells were distinguished from one another using fluorescence microscopy on the basis of the overall cell morphology and cell membrane integrity. Apoptotic cells show nuclear shrinkage, cytoplasmic membrane blebbing, but with membranes integrity. Necrotic cells show nuclear swelling and rupture of both nuclear and plasma membranes. AO can pass through the cell membrane, but EB cannot (Huang, Li, Liang, Yao, & Liu, 2011). Morphological changes were observed in the cells after treatment with different concentrations of PN50G for 48 h. A typical image of untreated cells with round, intact nuclei is shown in Fig. 3B(a) By contrast, apoptosis observed at the lower dose of 50 and 100 μg/mL (Fig. 3B(b and c) revealed marked nuclear condensation, membrane blebbing, and nuclear shrinkage, all of which are characteristics of apoptotic programmed cell death (as arrow illustrated). While at the higher dose, 200 μg/mL, necrosis was also observed (red).

3.4. Measurement of DNA damage by the comet assay

The comet assay is one of the most sensitive methods available for identifying breaks in the DNA strand. The extent of DNA damage was evaluated by the comet assay after incubating the A549 cells with or without PN50G (Fig. 4A). Significant PN50G-induced DNA damage was observed at the single-cell level. The length of the comet tail was significantly extended after treatment with 100 and 200 μg/ml PN50G ($P < 0.05$, $P < 0.01$, respectively) compared with that of the control (Fig. 4B).

3.5. Effect of PN50G on cell cycle distribution

Flow cytometry was performed with propidium iodide staining to quantitatively evaluate the PN50G-induced apoptosis. The cell percentages in the G_0/G_1, S, and G_2/M phases (Table 2) were calculated using the Multi-cycle software. The results show that treatments with different PN50G concentrations induced dose-dependent increases in the proportion of apoptotic cells in A549 (from 0.25% to 30.33%) and resulted in a significant accumulation of cells in the S phase (from 15.77% to 36.92%). The PN50G treatment for 48 h resulted in a dose-dependent decrease in the G2/M phase compared with that of the control (from 11.89% to 0.00%). The percentage of the G_0/G_1 phase in the treated cells decreased

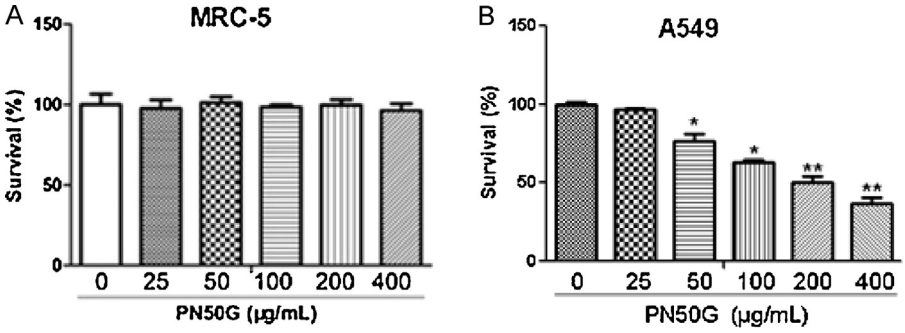

Fig. 2. (A) Effects of PN50G on the viability of non-tumor MRC-5 cells at different concentrations ($n = 6$). (B) Effects of PN50G on the viability of A549 cells at different concentrations ($n = 6$), $^*P < 0.05$, $^{**}P < 0.01$ vs. control.

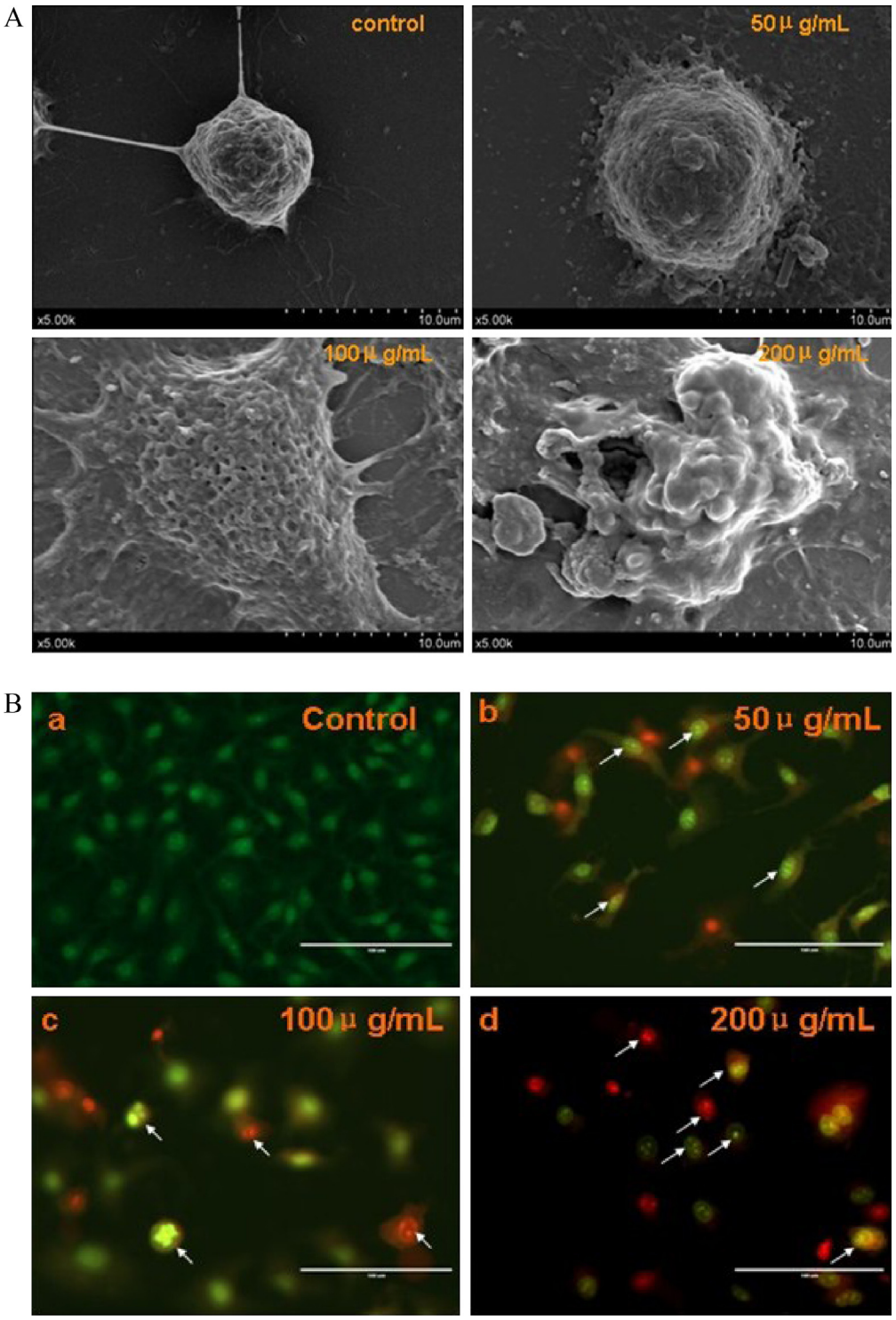

Fig. 3. (A) Scanning electron micrographs of macrophages treated with PN50G. Cells were prepared for SEM by treatment with 4% (v/v) glutaraldehyde for 2 h and 1% osmium tetroxide for 30 min. The osmium-fixed cells were then dehydrated with a graded ethanol series from 10% to absolute ethanol before air drying at room temperature and coated with gold. Original magnification ×5000. (B) Induction of PN50G on apoptotic body formation in A549 cells. The cells were treated with different doses of PN50G for 48 h and visualized for apoptotic bodies under fluorescent microscope (400×) using a blue filter after staining with AO/EB (scale bar: 100 μm).

relative to that of the control cells (from 72.34% to 33.07%). Apoptosis is an important cell biological characteristic. The results imply that PN50G-induced apoptosis is accompanied by cell cycle arrest in the S phase in cancer cells. This finding coincides with the hypothesis that PN50G acts as an S checkpoint that controls entry into the G_2 phase and prevents DNA replication (Vermeulen et al., 2003). These results all indicate that PN50G-induced cell death is principally due to apoptosis induction.

3.6. Analysis of mitochondrial membrane potential ($\Delta\Psi_m$) in A549 cells

The mitochondrial membrane potential ($\Delta\Psi_m$) of the cells was measured using the dye rhodamine-123 (Fig. 4C). A decrease in the mean fluorescence intensity was observed following cell treatment with PN50G. The bar graph represents the loss in $\Delta\Psi_m$ as a result of mitochondrial membrane depolarization, which is considered as

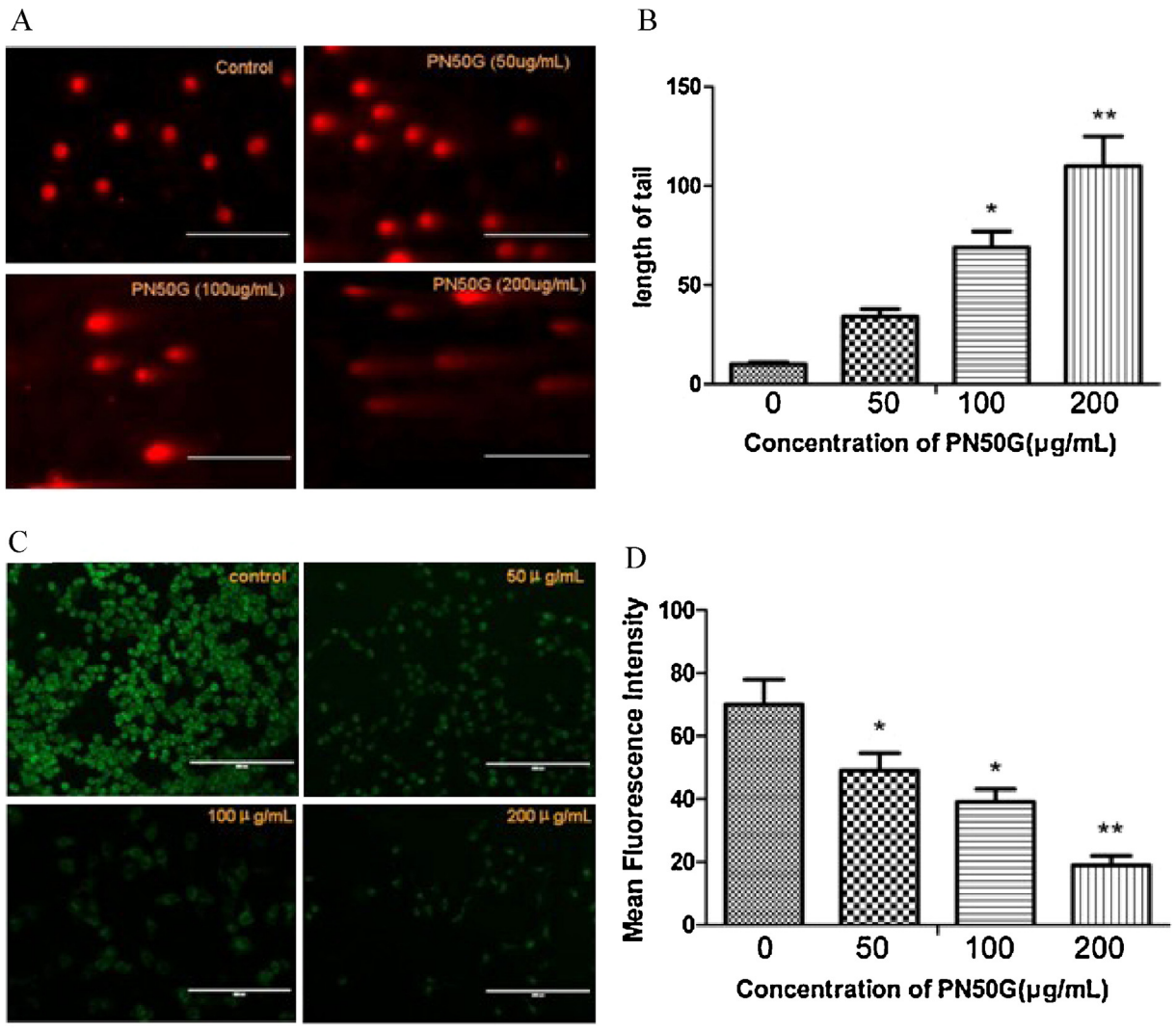

Fig. 4. (A) Comets were analyzed by confocal laser scanning microscopy at 543 nm (scale bar: 100 μm). (B) The length of comet tails increased in the presence of PN50G. (C) Loss of the mitochondrial membrane potential (DWm) (scale bar: 100 μm). (D) The mean fluorescence intensity of 20 cells selected at random was determined.

an initial and irreversible step of apoptosis (Adrie et al., 2001). The data indicate that PN50G-induced apoptosis was accompanied by changes in $\Delta\Psi_m$.

3.7. *Effects of PN50G on caspase-3 and caspase-9 gene expression*

An apoptosis executioner is responsible for the degradation of cellular proteins. Of these executioners, caspase-3 is activated by caspase-8 and/or caspase-9. We examined the mRNA expression of caspase-3 and caspase-9 to elucidate the mechanism underlying PN50G-induced apoptosis. qRT-PCR revealed that caspase-3 and caspase-9 expression significantly increased in the 200 μg/mL PN50G-treated group compared with that in the control cells (Fig. 5A and B). These results suggest that the increased expression of the caspase family contributes to the PN50G-induced apoptosis of A549 cells.

4. Discussion

Many chemotherapeutic agents exert their anticancer effects by inducing the apoptosis of cancer cells (Kamesaki, 1998). However, cancer chemotherapeutic agents also kill normal tissue cells, particularly blood cells and lymphocytes. Polysaccharides from edible fungi reportedly inhibit the proliferation of tumor cells (Ma et al., 2013; Xin et al., 2012). The present study demonstrated that the *P. nebrodensis* polysaccharide PN50G did not affect the proliferation viability of human fetal lung fibroblast cells MRC-5. However, the human non-small cell lung cancer A549 cell is an abnormal growth of cells that tend to proliferate in an uncontrolled way and is resistant to signals normally causing programmed cell death (apoptosis) (Silva, Rapior, Fons, Bahkali, & Hyde, 2012). PN50G induces cell growth inhibition in A549 cells by inducing apoptosis and cell cycle arrest as well as by activating a caspase cascade.

Mitochondrial permeability transition is a vital step in the induction of cellular apoptosis (Upur et al., 2011). The sequential activation of caspases is a key step in the execution phase of cell apoptosis. Most caspases regulate the apoptotic program through a caspase activation cascade that involves the initiators CASP-1, CASP-2, CASP-9, CASP-11, and CASP-12 and the effectors CASP-3 and CASP-7 (Garcia-Calvo et al., 1998; Ruiz-Vela, Opferman, Cheng, & Korsmeyer, 2005; Salvesen & Dixit, 1997), which crosstalk with CAPN-1 and CAPN-2 (Nakagawa et al., 2000; Ruiz-Vela, Gonzalez, Buitrago, & Martinez 1999).

We concluded that PN50G improves the immunity of RAW264.7 macrophages. PN50G appeared to activate tumor-inhibiting or killing processes through the activation of lymphocytes and

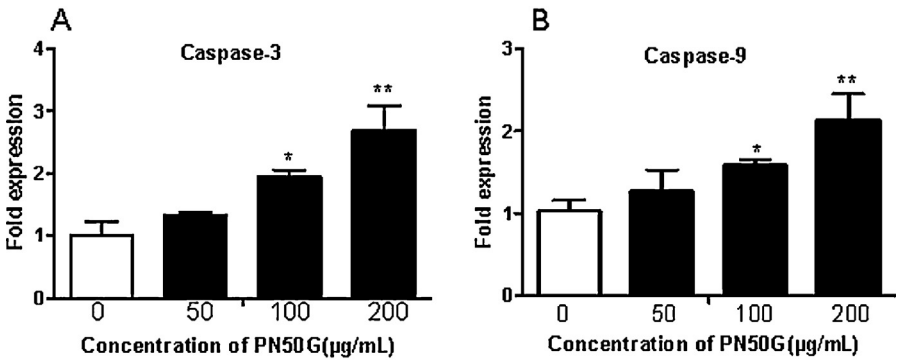

Fig. 5. (A) Caspase-3 mRNA expression of A549 cells treated with PN50G. (B) Caspase-9 mRNA expression of A549 cells treated with PN50G.

macrophages or cytokine (Wang et al., 2013). The induction of apoptosis possibly involve the regulation of c-Jun N-terminal kinase (Satomi, 2012), extracellular signal-regulated kinase (Takezawa, Okamoto, Nishio, Jänne, & Nakagawa 2011), Bcl-2 protein expression (Wang et al., 2012), and Akt signaling, as well as the inhibition of angiogenesis by suppressing the vascular endothelial growth factor expression and inhibition of cell transformation induced by the epidermal growth factor receptor (Kodama, Asakawa, Inui, Masuda, & Nanba, 2005). Therefore, the exact molecular mechanisms underlying PN50G-induced apoptosis remain unclear.

Our study demonstrated that a polysaccharide from *P. nebrodensis* inhibited the proliferation of tumor cells. This study highlights the potential of PN50G in cancer treatment. PN50G can be used included in the diet in the future to facilitate cancer treatment. However, the pleiotropic effects of PN50G on anticancer treatments and immunity improvement as well as its interrelations must still be investigated. Further in vivo studies must be conducted to evaluate the safety and efficacy of these polysaccharides in cancer patients.

Acknowledgment

We are grateful for the financial support provided by National Natural Science Foundation of China (Grant No. 31101357).

References

Adrie, C., Bachelet, M., Vayssier-Taussat, M., Russo-Marie, F., Bouchaert, I., Adib-Conquy, M., et al. (2001). Mitochondrial membrane potential and apoptosis peripheral blood monocytes in severe human sepsis. *Respiratory and Critical Care Medicine*, *164*, 389–395.

Bae, I. Y., Kim, H. Y., Lee, S., & Lee, H. G. (2011). Effect of the degree of oxidation on the physicochemical and biological properties of *Grifola frondosa* polysaccharides. *Carbohydrate Polymers*, *83*, 1298–1302.

Bremner, P., Rivera, D., Calzado, M. A., Obón, C., Inocencio, C., Beckwith, C., et al. (2009). Assessing medicinal plants from South-Eastern spain for potential antiinflammatory effects targeting nuclear factor-Kappa B and other proinflammatory mediators. *Journal of Ethnopharmacology*, *124*, 295–305.

Garcia-Calvo, M., Peterson, E. P., Leiting, B., Ruel, R., Nicholson, D. W., & Thornberry, N. A. (1998). Inhibition of human caspases by peptide-based and macromolecular inhibitors. *Journal of Biological Chemistry*, *273*, 32608–32613.

Hanif, R., Pittas, A., Feng, Y., Koutsos, H. I., Qiao, L., & Staiano-Coico, L. (1996). Effects of non-steroidal anti-inflammatory drugs on proliferation and on induction of apoptosis in colon cancer cells by a prostaglandin-independent pathway. *Biochemical Pharmacology*, *52*, 237–245.

Heo, S. J., Kim, K. N., Yoon, W. J., Oh, C., Choi, Y. U., Affan, A., et al. (2011). Chromene induces apoptosis via caspase-3 activation in human leukemia HL-60 cells. *Food and Chemical Toxicology*, *49*, 1998–2004.

Huang, H. L., Li, Z. Z., Liang, Z. H., Yao, J. H., & Liu, Y. J. (2011). Synthesis, cellular uptake, apopotosis, cytotoxicity, cell cycle arrest, interaction with DNA and antioxidant activity of ruthenium(II) complexes. *European Journal of Medicinal Chemistry*, *46*, 3282–3290.

Kamesaki, H. (1998). Mechanism involved in chemotherapy-induced apoptosis and their implications in cancer chemotherapy. *International Journal of Hematology*, *68*, 29–43.

Kodama, N., Asakawa, A., Inui, A., Masuda, Y., & Nanba, H. (2005). Enhancement of cytotoxicity of NK cells by D-fraction, a polysaccharide from *Grifola frondosa*. *Oncology Reports*, *13*, 497–502.

Lee, S.-M., Yoon, M.-Y., & Park, H.-R. (2008). Protective effects of *Paeonia lactiflora* pall on hydrogen peroxide-induced apoptosis in PC12 cells. *Bioscience, Biotechnology and Biochemistry*, *72*, 1272–1277.

Lemasters, J. J., & Nieminen, A. L. (1997). Mitochondrial oxygen radical formation during reductive and oxidative stress to intact hepatocytes. *Bioscience Reports*, *17*, 281–291.

Ma, L., Chen, H., Dong, P., & Lu, X. (2013). Anti-inflammatory and anticancer activities of extracts and compounds from the mushroom *Inonotus obliquus*. *Food Chemistry*, *139*, 503–508.

Miyazawa, N., Okazaki, M., & Ohga, S. (2008). Antihypertensive effect of *pleurotus nebrodensis* in spontaneously hypertensive rats. *Journal of Oleo Science*, *12*, 675–681.

Nakagawa, T., Zhu, H., Morishima, N., Li, E., Xu, J., Yankner, B. A., et al. (2000). Caspase-12 mediates endoplasmicreticulum- specific apoptosis and cytotoxicity by amyloid-beta. *Nature*, *403*, 98–103.

Newman, D. J., Cragg, G. M., & Snader, K. M. (2003). Natural products as sources of new drugs over the period 1981–2002. *Journal of Natural Products*, *66*, 1022–1037.

Parkin, D. M. (2001). Global cancer statistics in the year 2000. *Lancet Oncolology*, *2*, 533–543.

Ruiz-Vela, A., de Gonzalez, Buitrago, G., & Martinez, A. C. (1999). Implication of calpain in caspase activation during B cell clonal deletion. *EMBO Journal*, *18*, 4988–4998.

Ruiz-Vela, A., Opferman, J. T., Cheng, E. H., & Korsmeyer, S. J. (2005). Proapoptotic BAX and BAK control multiple initiator caspases. *EMBO Reports*, *6*, 379–385.

Salvesen, G. S., & Dixit, V. M. (1997). Caspases: Intracellular signaling by proteolysis. *Cell*, *91*, 443–446.

Satomi, Y. (2012). Fucoxanthin induces GADD45A expression and G1 arrest with SAPK/JNK activation in LNCap human prostate cancer cells. *Anticancer Research*, *32*, 807–813.

Schepetkin, I. A., & Quinn, M. T. (2006). Botanical polysaccharides: Macrophage immunomodulation and therapeutic potential. *International Immunopharmacology*, *6*, 317–333.

Silva, D. D., Rapior, S., Fons, F., Bahkali, A. H., & Hyde, K. D. (2012). Medicinal mushrooms in supportive cancer therapies: An approach to anti-cancer effects and putative mechanisms of action. *Fungal Diversity*, *55*, 1–35.

Takezawa, K., Okamoto, I., Nishio, K., Jänne, P. A., & Nakagawa, K. (2011). Role of ERK-BIM and STAT3-survivin signaling pathways in ALK inhibitor-induced apoptosis in EML4-ALK-positive lung cancer. *Clinical Cancer Research*, *17*, 2140–2148.

Thangam, R., Suresh, V., & Asenath Princy, W. (2013). C-Phycocyanin from *Oscillatoria tenuis* exhibited an antioxidant and in vitro antiproliferative activity through induction of apoptosis and G0/G1 cell cycle arrest. *Food Chemistry*, *140*, 262–272.

Upur, H., Yusup, A., Baudrimont, I., Umar, A., Berke, B., Yimit, D., et al. (2011). Inhibition of cell growth and cellular protein, DNA and RNA synthesis in human hepatoma (HepG2) cells by ethanol extract of abnormal Savda Munziq of traditional Uyghur medicine. *Evidence-Based Complementary and Alternative Medicine*, *25*, 14–24.

Vermeulen, K., Berneman, Z. N., & Van Bockstaele, D. R. (2003). Cell cycle and apoptosis. *Cell Proliferation*, *36*, 165–175.

Wang, C., Cui, H., Wang, Y., Wang, Z., Li, Z., Chen, M., et al. (2013). Bidirectional immunomodulatory activities of polysaccharides purified from *Pleurotus nebrodensis*. *Inflammation*, http://dx.doi.org/10.1007/s10753-013-9714-z

Wang, J., Chen, S., Xu, S., Yu, X., Ma, D., Hu, X., et al. (2012). In vivo induction of apoptosis by fucoxanthin, a marine carotenoid, associated with down-regulating STAT3/EGFR signaling in sarcoma 180 (S180) xenografts-bearing mice. *Marine Drugs*, *10*, 2055–2068.

Xie, J. H., Liu, X., Shen, M. Y., Nie, S. P., & Zhang, H. (2013). Purification, physicochemical characterisation and anticancer activity of a polysaccharide from *Cyclocarya paliurus* leaves. *Food Chemistry*, *136*, 1453–1460.

Xin, T., Zhang, F. B., Jiang, Q. Y., Chen, C. H., Huang, D. Y., Lv, Y. J., et al. (2012). A purification and antitumor activity of two acidic polysaccharides from the roots of *Polygala tenuifolia*. *Carbohydrate Polymers*, *90*, 1671–1676.